Intracellular Targeting

Deutsche Ausgabe: DOI: 10.1002/ange.201510142
Internationale Ausgabe: DOI: 10.1002/anie.201510142

Dual-Targeting Nanovesicles for In Situ Intracellular Imaging of and Discrimination between Wild-type and Mutant p53

*Ruocan Qian, Yue Cao, and Yi-Tao Long**

Abstract: *p53 is a tumor-suppressor protein related to the cell cycle and programmed cell apoptosis. Herein, dual-targeting nanovesicles are designed for in situ imaging of intracellular wild-type p53 (WTp53) and mutant p53 (MUp53). Nanovesicle-encapsulated plasmonic gold nanoparticles (AuNPs) were functionalized with consensus DNA duplexes, and a fluorescein isothiocyanate (FITC)-marked anti-MUp53 antibody was conjugated to the nanovesicle surface. After entering the cytoplasm, the released AuNPs aggregated through recognition of WTp53 and the double-stranded DNA. The color changes of AuNPs were observed using dark-field microscopy, which showed the intracellular WTp53 distribution. The MUp53 location was detected though the immunological recognition between FITC-labeled anti-MUp53 and MUp53. Thus, a one-step incubation method for the in situ imaging of intracellular WTp53 and MUp53 was obtained; this was used to monitor the p53 level under a drug treatment.*

Human p53 is a tumor suppressor protein that inhibits tumor progression through control of the cell cycle and programmed cell apoptosis.[1] Human wild-type p53 protein (WTp53) contains a central specific DNA-binding domain.[2] which is able to bind a consensus-site double-stranded DNA (ds-DNA). The central specific DNA-binding domain contains at least two copies of the 10 base pair (bp) half site with a sequence of PuPuPuC(A/T)(T/A)GPyPyPy (Pu = purine, and Py = pyrimidine).[3] In most types of cancer cells, the central DNA-binding domain of the p53 protein is mutated and loses its binding ability because of extensive mutation of the p53 gene.[4] The abnormal expression of mutant p53 protein (MUp53) has been regarded as an important stimulus for carcinogenesis.[5] Therefore, the detection of and discrimination between WTp53 and MUp53 are of great significance in cancer diagnosis.

Thus far, various strategies have been reported for detecting endogenous p53, including enzyme-linked immunosorbent assay (ELISA),[6] immunohistochemistry methods,[7] electrophoretic mobility shift assay,[8] and ds-DNA consensus binding-based biosensing.[1a,b,9] The most widely used method is ELISA, which is sensitive but only measures the total p53 (WTp53 and MUp53 combined). Therefore, Wang et al. developed a consensus ds-DNA modified electrode for the simultaneous analysis of WTp53 and total p53 in cell lysates.[1] Despite the satisfactory sensitivity and detection limit of these methods, most of them use cell lysates as samples and, thus, fail to provide the p53 location and distribution information at the single-cell level. Therefore, there is a need to develop in situ strategies for analyzing intracellular p53.

Recently, plasmonic nanoparticles, especially gold nanoparticles (AuNPs), have attracted significant attention owing to their optical and physical properties, which provide the capability to absorb and scatter visible light, which induces localized surface-plasmon resonance (LSPR).[10] With the development of dark-field microscopy (DFM) and plasmon-resonance Rayleigh scattering (PRRS) spectroscopy, plasmonic nanoparticles have been successfully used in biosensing,[11] single-particle analysis,[12] and intracellular monitoring.[13] Inspired by the plasmonic properties of AuNPs and their excellent biocompatibility,[10b,14] we designed a plasmonic AuNP that was functionalized with a consensus ds-DNA (AuNP/CDNA) that recognizes WTp53. After the encapsulation of the AuNPs in a liposome[15] a fluorescein isothiocyanate (FITC)-marked *anti*-MUp53 antibody was used to modify the surface of the liposome through a stable oxime linkage with the inserted undecanal;[16] thus, dual-targeting nanovesicles were generated for the in situ imaging and non-invasive detection of both WTp53 and MUp53 in single cells (Scheme 1). The ds-DNA on the surface of the AuNPs contained consensus sequences to recognize and bind to WTp53. The resulting interaction of WTp53 tetramers and

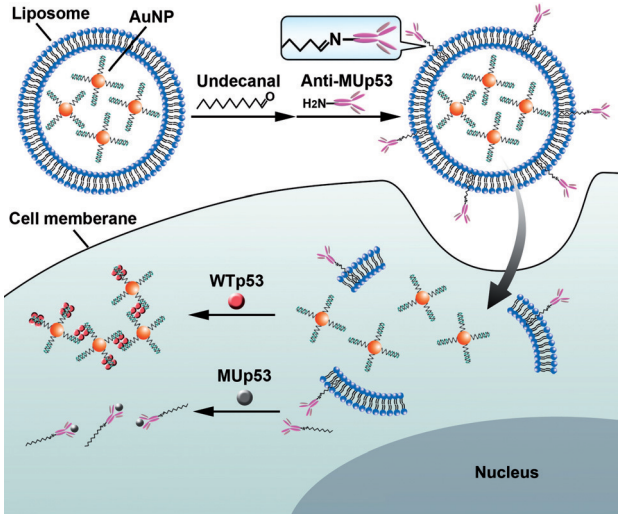

Scheme 1. A schematic illustration of a dual-targeting nanovesicle for in situ analysis of intracellular WTp53 and MUp53.

[*] R. Qian, Y. Cao, Prof. Y.-T. Long
Key Laboratory for Advanced Materials
East China University of Science and Technology
Shanghai, 200237 (P.R. China)
E-mail: ytlong@ecust.edu.cn

Supporting information for this article is available on the WWW under http://dx.doi.org/10.1002/anie.201510142.

AuNPs induced AuNP aggregation, which caused color changes in DFM. To detect p53 in living cells, the AuNP/CDNA-encapsulated and antibody-modified liposome was transported into the cytoplasm to release the AuNP/CDNA and *anti*-MUp53. The intracellular WTp53 triggered the aggregation of AuNP/CDNA and, thus, induced changes in light scattering, which were detected using the DFM imaging. The intracellular MUp53 was detected using the FITC-labeled anti-MUp53 and was observed through the fluorescence signal. Therefore, WTp53 and MUp53 were simultaneously imaged.

AuNPs were prepared using a reported seed-growing method.[17] AuNP/CDNA was obtained by incubating AuNPs with the DNA oligonucleotides O1 and their complementary sequence O2 (used to form consensus ds-DNA). A transmission electron microscopy (TEM) image of the AuNPs showed an average diameter of 60 nm with a homogeneous distribution (Figure 1 a). The UV/Vis spectrum of the AuNP/CDNA showed a characteristic DNA peak at 260 nm (Figure 1 b), which demonstrated the successful modification of the ds-DNA with AuNPs. As shown in Figure 1 c, AuNPs were observed as green spots in the DFM image. The color of the spots did not change after the ds-DNA modification (Figure 1 d), suggesting that the diameters of the AuNP/CDNA diameter and the bare AuNPs were identical. A DFM image of the nanovesicles showed dispersed groups of AuNP/CDNA, indicating the formation of AuNP/CDNA-encapsulated liposomes (Figure 1 e). Successful conjugation of anti-MUp53/FITC was observed in the corresponding fluorescence image (Figure 1 f).

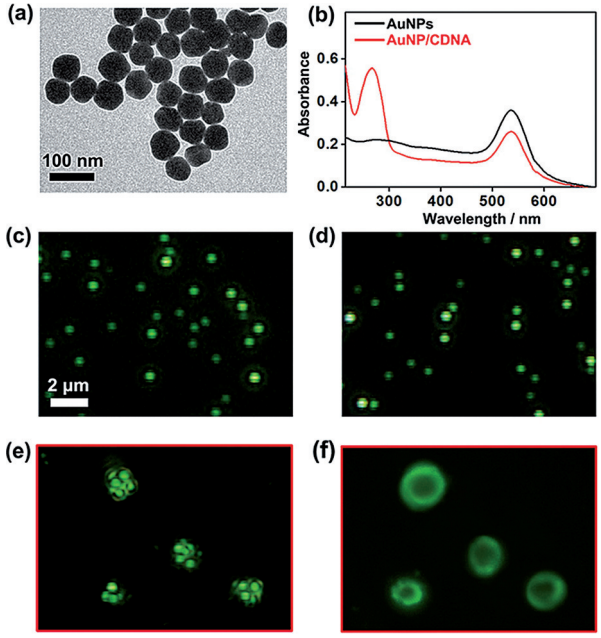

Figure 1. a) TEM image of the prepared AuNPs. b) UV/Vis spectra of AuNPs and AuNP/CDNA. Dark-field microscopy images of c) AuNPs, d) AuNP/CDNA, and e) nanovesicles. f) Fluorescence image of nanovesicles. The scale in (c), (d), (e), and (f) is the same.

To test the response of AuNP/CDNA to WTp53, DFM images of the AuNP/CDNA and WTp53 mixtures were recorded after different incubation times (Supporting Information, Figure S2). The color of the AuNP/CDNA gradually changed from green to orange with increasing incubation times and showed little further change after 90 min, which demonstrated the WTp53-triggered aggregation of AuNP/CDNA. With the optimized reaction time, the AuNP/CDNA was incubated with a series of WTp53 solutions of different concentrations. As shown in Figure 2 a, at a low WTp53 concentration, the AuNP/CDNA color was green, and the scattering spectrum peak was almost identical to that of the control (Figure 2 a, i1–i2). The color gradually became yellow and then orange as the WTp53 concentration increased, and the scattering spectral peak shifted from 559 nm to 650 nm upon the WTp53 and AuNP/CDNA conjugation (Figure 2 a, i2–i7). Therefore, a convenient quantification method for WTp53 was established based on DFM images that were obtained using different concentrations of WTp53-treated AuNP/CDNA. From the DFM images (Supporting Information, Figure S3), the average ratio of the red channel intensity to the green channel intensity (R/G) of the AuNP/CDNA was determined using Adobe Photoshop software (Figure 2 b). Thus, a calibration curve was obtained, which showed a linear relationship between the R/G value and the WTp53 concentration (Figure 2 b, inset). The detection limit was calculated to be 0.01 μM.

Before the intracellular detection, HeLa cell extracts were used to test the feasibility of the AuNP/CDNA-based method. A p53-promoting drug, nutlin-3,[18] was used as a model drug to study the changes in the p53 level in HeLa cells. After HeLa cells (1 mL, 1×10^6 mL^{-1}) were incubated with different amounts of nutlin-3 for 48 h, the cell extracts were added to AuNP/CDNA and then incubated for DFM imaging (Figure 3 a). The DFM images showed a color change from green to orange as the amount of drug increased; this finding indicated an increase in the WTp53 level with nutlin-3 treatment. To measure the level of total p53 (WTp53 and MUp53), a p53 pan ELISA kit (HaoChen Biotech. Co. Ltd. Shanghai, China) was applied to test the cell extracts, and the standard calibration curve was established (Supporting Information, Figure S5). As shown in Figure 3 b, the total p53 level increased with drug treatment, whereas a gradual decline was observed in the MUp53 level, which indicated nutlin-3′s ability to regulate p53 expression.

To demonstrate that AuNPs could protect consensus ds-DNA, the supernatant of the acidic AuNP/CDNA solution (pH was adjusted to 6.0), which was incubated with the HeLa cell extract, was collected for UV/Vis measurement. The spectrum of the supernatant showed no characteristic peak from DNA at 260 nm (Supporting Information, Figure S6), indicating that AuNPs could adequately protect the DNA structure that was bound on the surface.

The specificity of the consensus ds-DNA recognition of WTp53 was tested using a control experiment. A pair of control DNA samples was used to prepare nonconsensus ds-DNA-modified AuNPs, which were used for the same WTp53 incubation test with DFM imaging. After 90 min of incubation, the nonconsensus ds-DNA-modified AuNPs showed

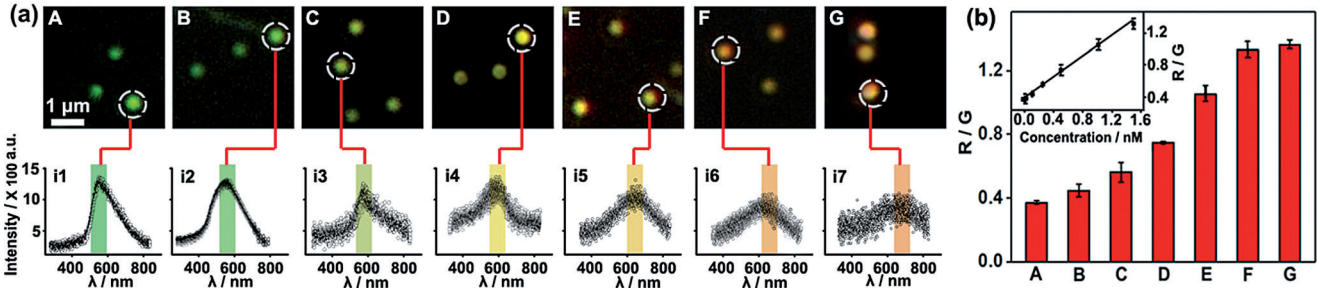

Figure 2. a) DFM images of 20 μL AuNP/CDNA incubated with 5 μL WTp53 for 90 min with different concentrations (final WTp53 concentration: control, 0.01, 0.1, 0.25, 0.5, 1.0, and 1.5 μM from (A) to (G). i1)–i7): Corresponding scattering spectra of AuNP/CDNA observed in DFM images. b) Average R/G value of AuNP/CDNA incubated with different concentrations of WTp53 (control, 0.01, 0.1, 0.25, 0.5, 1.0, and 1.5 μM from (A) to (G); Inset: Standard curve for in vitro detection of WTp53 by DFM imaging (R/G data were collected from at least 10 AuNP/CDNA dots, see Supporting Information, Figure S3).

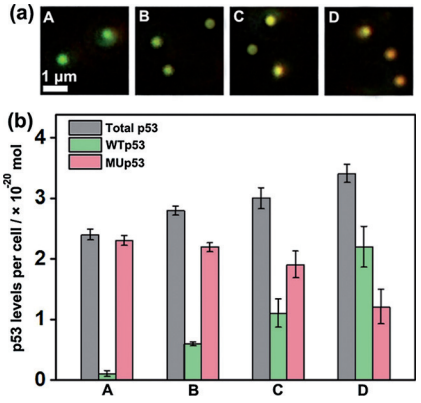

Figure 3. a) DFM images of 20 μL AuNP/CDNA incubated with 5 μL HeLa cell extract (treated with 0, 62.5, 125, and 250 μg mL^{-1} nutlin-3 from (A) to (D)) for 90 min. b) P53 levels (total p53, WTp53, and MUp53) in a single HeLa cell (detected from cell extracts collected from HeLa cells treated with: no, 62.5, 125, 250 μg mL^{-1} nutlin-3 from (A) to (D)).

a similar green color and scattering peak as those of the control (Supporting Information, Figure S7 A), which confirmed the specific conjugation between the consensus ds-DNA and WTp53. In addition, BSA and MUp53 were mixed with the AuNP/CDNA respectively, and neither of them induced aggregation (Supporting Information, Figure S7 B,C).

Prior to cell imaging, the cytotoxicity of AuNP/CDNA was examined using an MTT assay. HeLa cells were incubated with AuNP/CDNA for various times, and the absorbances were measured to determine the relative cell viability. After 4 h of incubation, the cells remained active with 90 % cell viability (Supporting Information, Figure S8), which demonstrated the good biocompatibility of AuNP/CDNA during the cell test.

For intracellular detection, HeLa cells (1 mL, 1×10^6 mL^{-1}) were seeded in a culture dish. After the addition of 60 μL of the AuNP-wrapped nanovesicles, DFM images were acquired at different times. For the first 30 min, only a few AuNP/CDNA particles were observed. After 1 h, significantly more AuNP/CDNA particles appeared around the nucleus and were dispersed in the cytoplasm. The number of AuNP/CDNA grew with incubation time until a plateau was reached after 2 h (Supporting Information, Figure S9).

For this optimal incubation time of 2 h, the nanovesicles and DAPI-incubated HeLa cells were analyzed in detailed using DFM imaging, fluorescent imaging, and scattering spectra scanning (Figure 4). As shown in Figure 4, A1–A5, the AuNP/CDNA had a greenish color, and the scattering spectra had a peak at approximately 570 nm (Figure 4, i1–i3), which indicated a low WTp53 level in the HeLa cells. However, the anti-MUp53/FITC fluorescence image showed an extensive distribution of MUp53 in the cytoplasm (Figure 4, A4). The p53 regulation effect of nutlin-3 was further explored in HeLa cells (1 mL, 1×10^6 mL^{-1}) that were treated with different amounts of nutlin-3 for 48 h. After 2 h of incubation with 60 μL of the nanovesicles, the cells were imaged microscopically, and the scattering spectra were collected. With increasing doses of nutlin-3, the color of AuNP/CDNA became orangish in the DFM images (Figure 4, B1, C1, D1), and the scattering peak gradually redshifted from 585 nm to 650 nm (Figure 4, i4–i12); these changes suggested a dose-dependent increase in intracellular WTp53 by nutlin-3. Meanwhile, the fluorescence intensity of anti-MUp53/FITC decreased, which indicated the inhibition of MUp53 by the drug treatment (Figure 4, B4, C4, and D4). Thus, the nanovesicles could be used to obtain intracellular images of WTp53 and MUp53.

In addition, a control experiment was performed to demonstrate the advantage of using liposomes for intracellular delivery. HeLa cells that were treated with AuNP/CDNA but without liposome, had fewer AuNPs in the cytoplasm, as indicated by DFM observation, than those found in the observations that used nanovesicles (Supporting Information, Figure S10), which indicated a high nanovesicle internalization efficiency. The uptake efficiency was reduced at a lower temperature (Supporting Information, Figure S11 a), showing an energy-dependent endocytosis of the nanovesicles. After entering cells, the nanovesicles were wrapped by the lysosomes and then the AuNPs quickly escaped from the lysosomes into the cytoplasm (Supporting Information, Figure S11 b,c), possibly a result of lipid-membrane fusion between the lysosomal membrane and the liposomal wall of the nanovesicles. These results suggested that the proposed nanostructure could be successfully used as trans-membrane delivery vehicles.

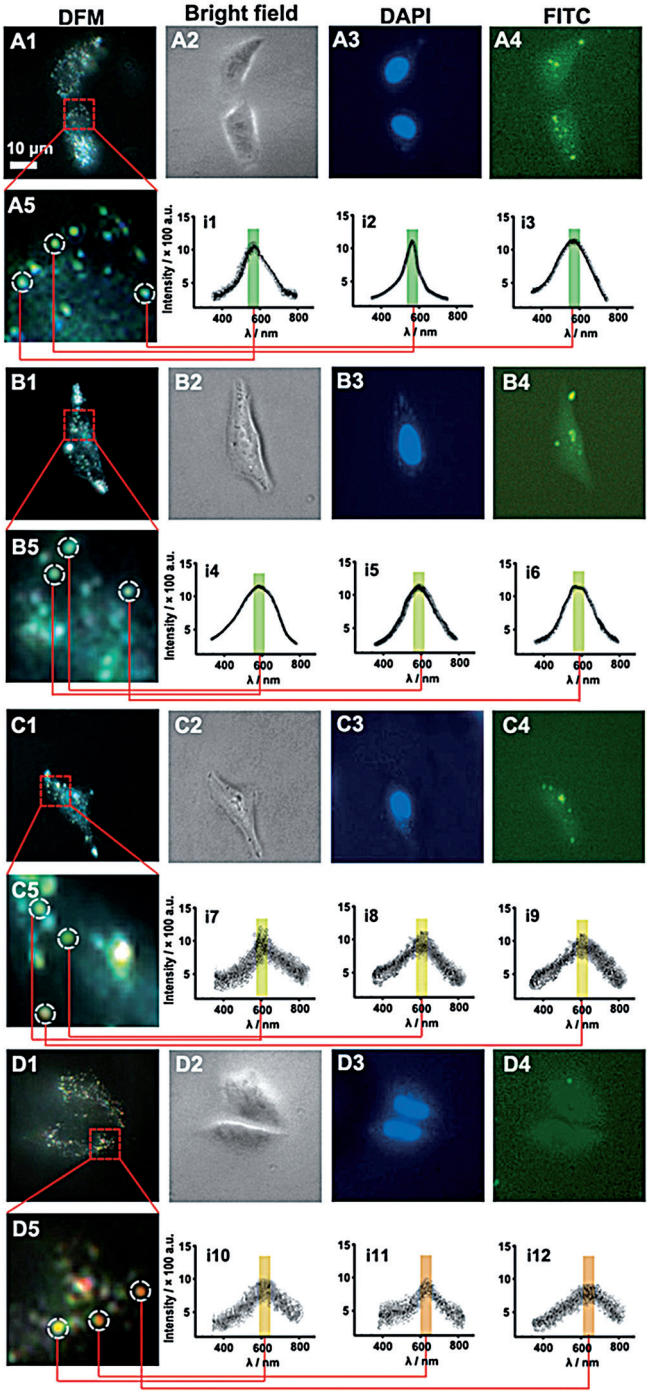

Figure 4. Microscopic images of HeLa cells treated with different amounts of nutlin-3 (A1–A5: control, B1–B5: 62.5 μg mL^{-1}, C1–C5: 125 μg mL^{-1}, D1–D5: 250 μg mL^{-1}) and then incubated with nanovesicles and DAPI for 2 h (1: DFM image, 2: bright field image, 3: DAPI stained nucleuses, 4: FITC marked MUp53, 5: the detail view of HeLa cell containing AuNP/CDNA). i1–i12: Corresponding scattering spectra of AuNP/CDNA in HeLa cells.

In conclusion, this work designed dual-targeting nanovesicles for the in situ intracellular imaging of WTp53 and MUp53. The plasmonic AuNP/CDNA developed was easy to prepare and had good cytocompatibility, intracellular stability, and WTp53 specificity. The AuNP-wrapped and anti-MUp53/FITC-modified nanovesicles readily entered living cells to release AuNP/CDNA and anti-MUp53/FITC. The conjugation of AuNP/CDNA and WTp53 caused a color change, which was observed with DFM, whereas the MUp53 was marked with anti-MUp53/FITC and generated a fluorescence image. Thus, the intracellular imaging of p53 was achieved using a one-step incubation with nanovesicles. The developed method is suitable for monitoring changes in the intracellular p53 level during p53-related drug treatments, which can help to elucidate the role of p53 in the biological events of a cell. Therefore, this capability indicates the usefulness of the method for cancer diagnosis and monitoring.

Acknowledgements

This research was supported by the National Natural Science Foundation of China (21327807), the Science Fund for Creative Research Groups (21421004), the National Science Fund for Distinguished Young Scholars of China (21125522), and the China Postdoctoral Science Foundation (2015M570335).

Keywords: dual targeting · fluorescence imaging · nanovesicles · plasmonic imaging · p53

How to cite: *Angew. Chem. Int. Ed.* **2016**, *55*, 719–723
Angew. Chem. **2016**, *128*, 729–733

[1] a) J. X. Wang, X. Zhu, Q. Y. Tu, Q. Guo, C. S. Zarui, J. Momand, X. Z. Sun, F. M. Zhou, *Anal. Chem.* **2008**, *80*, 769–774; b) Y. C. Wang, X. Zhu, M. H. Wu, N. Xia, J. X. Wang, F. M. Zhou, *Anal. Chem.* **2009**, *81*, 8441–8446; c) B. Vogelstein, D. Lane, A. J. Levine, *Nature* **2000**, *408*, 307–310.

[2] a) K. Iwabuchi, P. L. Bartel, B. Li, R. Marraccino, S. Fields, *Proc. Natl. Acad. Sci. USA* **1994**, *91*, 6098–6102; b) T. Kanda, K. Segawa, N. Ohuchi, S. Mori, Y. Ito, *Mol. Cell. Biol.* **1994**, *14*, 2651–2663; c) T. Unger, J. A. Mietz, M. Scheffner, C. L. Yee, P. M. Howley, *Mol. Cell. Biol.* **1993**, *13*, 5186–5194.

[3] a) P. Wang, M. Reed, Y. Wang, G. Mayr, J. E. Stenger, M. E. Anderson, J. F. Schwedes, P. Tegtmeyer, *Mol. Cell. Biol.* **1994**, *14*, 5182–5191; b) Y. Wang, F. J. Schwedes, D. Parks, K. Mann, P. Tegtmeyer, *Mol. Cell. Biol.* **1995**, *15*, 2157–2165; c) N. P. Pavletich, K. A. Chambers, C. O. Pabo, *Genes Dev.* **1993**, *7*, 2556–2564; d) T. Gohler, S. Jager, G. Warnecke, H. Yasuda, E. Kim, W. Deppert, *Nucleic Acids Res.* **2005**, *33*, 1087–1100; e) M. Reed, B. Woelker, P. Wang, Y. Wang, M. E. Anderson, P. Tegtmeyer, *Proc. Natl. Acad. Sci. USA* **1995**, *92*, 9455–9459.

[4] a) A. J. Levine, *Cell* **1997**, *88*, 323–331; b) D. Hamroun, S. Kato, C. Ishioka, M. Claustres, C. Beroud, T. Soussi, *Hum. Mutat.* **2006**, *27*, 14–20; c) A. J. Levine, C. A. Finlay, P. W. Hinds, *Cell* **2004**, *116*, S67–S69; d) T. Soussi, C. Ishioka, M. Claustres, C. Béroud, *Nat. Rev. Cancer* **2006**, *6*, 83–90; e) T. Soussi, J. M. Rubio-Nevado, C. Ishioka, *Hum. Mutat.* **2006**, *27*, 1151–1154.

[5] a) L. Bai, W. Zhu, *J. Cancer Mol.* **2006**, *2*, 141–153; b) C. Xiang, C. Shen, Z. Wu, Y. Qin, Y. Zhang, C. Liu, J. Chen, S. Zhang, *J. Occup. Health* **2007**, *49*, 279–284.

[6] a) E. Jagelská, V. Brázda, S. Pospisilová, B. Vojtesek, E. Palecek, *J. Immunol. Methods* **2002**, *267*, 227–235; b) K. A. Gould, C. Nixon, M. J. Tilby, *Mol. Pharmacol.* **2004**, *66*, 1301–1309.

[7] a) I. I. Wistuba, A. F. Gazdar, I. Roa, J. Albores-Saavedra, *Hum. Pathol.* **1996**, *27*, 360–365; b) E. T. M. A. Gaballah, M. A. Tawfik, *Saudi Dent. J.* **2010**, *22*, 167–170; c) M. H. Bukhari, S.

Niazi, M. Anwar, N. A. Chaudhry, S. Naeem, *Ann. N. Y. Acad. Sci.* **2008**, *1138*, 1 – 9.
[8] a) Y. Adachi, W. Chen, H. S. Wei, T. Kamata, *Anal. Biochem.* **2005**, *342*, 348 – 351; b) I. Beno, K. Rosenthal, M. Levitine, L. Shaulov, T. E. Haran, *Nucleic Acids Res.* **2011**, *39*, 1919 – 1932.
[9] X. L. Chen, C. H. He, Z. F. Zhang, J. X. Wang, *Biosens. Bioelectron.* **2013**, *47*, 335 – 339.
[10] a) J. N. Anker, W. P. Hall, O. Lyandres, N. C. Shah, J. Zhao, R. P. VanDuyne, *Nat. Mater.* **2008**, *7*, 442 – 453; b) S. Eustis, M. A. El-Sayed, *Chem. Soc. Rev.* **2006**, *35*, 209; c) K. R. Catchpole, A. Polman, *Opt. Express* **2008**, *16*, 21793 – 21800; d) K. M. Mayer, J. H. Hafner, *Chem. Rev.* **2011**, *111*, 3828.
[11] Y. Li, C. Jing, L. Zhang, Y. T. Long, *Chem. Soc. Rev.* **2012**, *41*, 632 – 642.
[12] a) L. X. Qin, C. Jing, Y. Li, D. W. Li, Y. T. Long, *Chem. Commun.* **2012**, *48*, 1511 – 1513; b) Q. Liu, C. Jing, X. X. Zheng, Z. Gu, D. Li, D. W. Li, Q. Huang, Y. T. Long, C. H. Fan, *Chem. Commun.* **2012**, *48*, 9574 – 9576.
[13] C. Jing, Z. Gu, Y. L. Ying, D. W. Li, L. Zhang, Y. T. Long, *Anal. Chem.* **2012**, *84*, 4284 – 4291.
[14] D. S. Seferos, D. A. Giljohann, H. D. Hill, A. E. Prigodich, C. A. Mirkin, *J. Am. Chem. Soc.* **2007**, *129*, 15477 – 15479.
[15] B. Dalby, S. Cates, A. Harris, E. C. Ohki, M. L. Tilkins, P. J. Price, V. C. Ciccarone, *Methods* **2004**, *33*, 95 – 103.
[16] M. M. Elmi, M. N. Sarbolouki, *Int. J. Pharm.* **2001**, *215*, 45 – 50.
[17] a) K. C. Grabar, R. G. Freeman, M. B. Hommer, M. J. Natan, *Anal. Chem.* **1995**, *67*, 735 – 743; b) S. Link, M. A. El-Sayed, *J. Phys. Chem. B* **1999**, *103*, 4212 – 4217.
[18] L. T. Vassilev, B. T. Vu, B. Graves, D. Carvajal, F. Podlaski, Z. Filipovic, N. Kong, U. Kammlott, C. Lukacs, C. Klein, N. Fotouhi, E. A. Liu, *Science* **2004**, *303*, 844 – 848.

Received: October 31, 2015
Published online: November 27, 2015

